Applied Physics Express **5** (2012) 041102
DOI: 10.1143/APEX.5.041102

High-Work-Function Transparent Conductive Oxides with Multilayer Films

Chunyan Song[1,2], Hong Chen[3], Yi Fan[1], Jinsong Luo[1], Xiaoyang Guo[1]*, and Xingyuan Liu[1]*

[1]*State Key Laboratory of Luminescence and Applications, Changchun Institute of Optics, Fine Mechanics and Physics, Chinese Academy of Sciences, Changchun 130033, China*
[2]*Graduate School of Chinese Academy of Sciences, Beijing 100039, China*
[3]*Key Laboratory of Optical System Advanced Manufacturing Technology, Chinese Academy of Sciences, Changchun 130033, China*

Received January 3, 2012; accepted March 5, 2012; published online March 22, 2012

Transparent conductive oxide (TCO) films using WO_3/Ag/WO_3 (WAW) were fabricated under room temperature conditions. WAW has a low sheet resistance of 12 Ω/sq and a work function of 6.334 eV. This is one of the TCOs with the highest work function. These properties make it useful for application in electroluminescent devices and solar cells. Both theoretical calculation and experimental results show that the two WO_3 layers strongly affect transparency, while the Ag layer determines transmittance and electrical performances. These rules can be applied in all dielectric/metal/dielectric structures. © 2012 The Japan Society of Applied Physics

Transparent conductive oxide (TCO) films are critical components in flat-panel displays, solar cells, gas sensors, and smart windows.[1–4] As transparent electrodes in optoelectronic devices, TCOs are responsible for carrier injection in electroluminescent devices or carrier extraction in solar cells. In organic light-emitting devices (OLEDs), the high-work-function of TCOs can reduce the barrier height at the anode/hole transport layer interface, and can improve hole injection efficiency.[5] Sn-doped In_2O_3 (ITO) is the most commonly used TCO in optoelectronic devices.[6–8] However, its work function (4.7–4.9 eV) is much lower than the highest occupied molecular orbital level of most hole transport materials in OLEDs.[9] Most reported TCO work functions are in the range of 4 to 5 eV.[3,10] The highest work function of TCO of 6.1 eV was reported by Cui *et al.*[11,12]

Indium, the main component of ITO, is becoming more difficult to obtain. Therefore there has been extensive research into low-indium or indium-free TCOs. Dielectric–metal–dielectric (DMD) is a special kind of TCO which has attracted attention due to its low sheet resistance, high transmittance in the visible region, and its simple fabrication process. Metals like Ag, Au, and Cu (especially Ag), and various dielectrics such as SnO_2, ZnS, and TiO_2 have been introduced in the DMD structure.[3,13] Transparency and conductivity are two primary properties of TCOs. However, how each layer influences DMD properties like transmittance, sheet resistance, and mobility are not well understood. Recently, WO_3/Ag/WO_3 (WAW) has been used as cathodes in top-emitting OLEDs.[14,15] Generally, an effective cathode in OLEDs should have a low work function. WO_3 has a low valence band level of 7.94 eV and an energy gap (E_g) of 2.7–3.3 eV,[16,17] and Ag has a high work function of 4.52–4.74 eV.[18] In addition, many reports have shown that adopting a WO_3 interlayer as a hole injection layer can improve the OLED efficiency.[19,20] In this study we investigate whether WAW is a high-work-function TCO, which can be better used as an anode in OLEDs. We report the transparent and conductive properties of WAW films. Theoretical calculations are given on how each layer affects WAW transmittance. Moreover, the optimal layer thicknesses of WAW are provided.

The WAW films were created on a precleaned polished glass substrate by e-beam evaporation under room temperature. The thicknesses of the WO_3 and Ag layers varied between 27–40 and 7–22 nm, respectively. For both WO_3 layers, O_2 gas was introduced upstream at 15–16.9 sccm to ensure that the vacuum pressure was $1.9–2.2 \times 10^{-2}$ Pa. The evaporation rate of the WO_3 material was about 0.06–0.1 nm/s. The Ag material was evaporated below 1.0×10^{-3} Pa with a rate of 0.2–1.4 nm/s. Sheet resistances were measured using a four-probe method. The carrier concentration and Hall mobility of the WAW films were determined using a HMS-3000 Hall effect measurement system with an applied magnetic filed of 0.55 T. The surface work function of the WAW films was measured using a KP Technology Ambient Kelvin probe system package. Film thicknesses were calibrated with an Ambios XP-1 surface profiler. The transmittance spectra of WAW samples were recorded using a Shimadzu UV-3101PC spectrophotometer. All the measurements were performed at room temperature.

WO_3, with a refractive index of 2.2, is nonabsorbing in the region of 400–2000 nm. The characteristic matrix of WAW on a glass substrate is[21]

$$\begin{bmatrix} B \\ C \end{bmatrix} = \left\{ \prod_{j=1}^{3} \begin{bmatrix} \cos\delta_j & \frac{i}{\eta_j}\sin\delta_j \\ i\eta_j \sin\delta_j & \cos\delta_j \end{bmatrix} \right\} \begin{bmatrix} 1 \\ \eta_4 \end{bmatrix}, \quad (1)$$

$$\eta_j = \begin{cases} N_j/\cos\theta_j & \text{for p-polarized wave} \\ N_j\cos\theta_j & \text{for s-polarized wave} \\ N_j & \text{for normal light incidence} \end{cases}, \quad (2)$$

where $j = 0$ (for incidence medium); 1, 2, or 3 for DMD layers; or 4 for the substrate layer. The angular phase thickness is $\delta_j = (2\pi/\lambda)N_j d_j \cos\theta_j$. θ_j is the angle of wave propagation in the layer as determined from Snell's law. N_j denotes the refractive index of each layer, which is relevant to the incident wavelength λ. The physical thicknesses of the plate WO_3 exposed to air, the Ag plate, and the WO_3 plate on the glass substrate are represented by d_1, d_2, and d_3, respectively. The transmittance can be given as

$$T = \frac{4\eta_0\eta_4}{(\eta_0 B + C)^2}. \quad (3)$$

Here, we only consider vertical incidence, thus, $\delta_j = (2\pi/\lambda)N_j d_j$, and $\eta_j = N_j$. Using data of Ag from the literature,[18] we can simulate transmittance for WAW with glass $N_4 = 1.52$ as a substrate and under vertical incidence, by inputting $j = 1, 2, 3$, $N_1 = 2.2$, $N_2 = n_2(\lambda) - ik_2(\lambda)$, $N_3 = 2.2$, $N_4 = 1.52$ using a computer.

*E-mail address: liuxy@ciomp.ac.cn

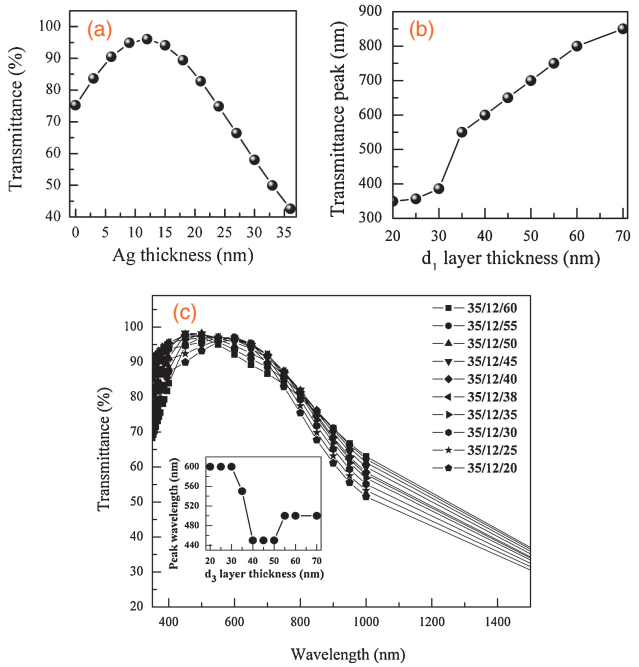

Fig. 1. Simulation graphs of WAW. (a) Average transmittance of WAW ($35/x/35$ nm) in the visible region under different Ag thicknesses, where $x = 0, 3, 6, \ldots, 36$ nm. For d_1 and d_3 (WO_3) layers, the thicknesses of WAW were set to $x/12/35$ nm and $35/12/x$ nm, respectively. The transmittance properties were simulated with $x = 20, 25, \ldots, 70$ nm. (b) Dependence of WAW transmittance peak on the thickness of d_1 layer. (c) Dependence of WAW transmittance spectra and transmittance peak (inset) on the thickness of d_3 layer.

We studied the effect of d_1, d_2, and d_3 layers on WAW transmittance in the visible region. We simulated WAW ($35/x/35$ nm) transmittance with different d_2 (Ag) layer thickness (from 0 to 36 nm). As shown in Fig. 1(a), the average transmittance of WAW in the visible region is strongly related to the Ag layer thickness. The optimum thickness is 12 nm; at this point either increasing or decreasing the Ag layer thickness decreases WAW transmittance. Figure 1(b) shows that the transmittance peak reveals a red-shift with the increase of d_1 thickness from 20 to 70 nm. However, the shift of the transmittance peak is not regular with the thickness increase of the d_3 layer [inset of Fig. 1(c)]. Furthermore, Fig. 1(c) indicates a blue shift of the high-transmittance region. The experimental data followed the simulated data closely, but not exactly, because of the varied optical constants of WO_3 and Ag films during the deposition process.[22)]

We fabricated WAW (36/11/38 nm, in total 85 nm) and single layers of Ag (11 nm) and WO_3 (74 nm) on glass substrates, separately. Their transmittance spectra are shown in Fig. 2. In the visible region, the single-layer Ag has a low average transmittance of 37.8%, while the WO_3 layer has an average transmittance of 84.6%. The three-layer WAW has an average transmittance of 81.3% and a peak transmittance of 88%. The transmittance of WAW in part of the visible region is higher than that of either the single WO_3 layer or the Ag layer (Fig. 2). This is because the total transmittance of WAW is not determined only by one or two layers, but by all of the layers together with the substrate according to the characteristic matrix of WAW.

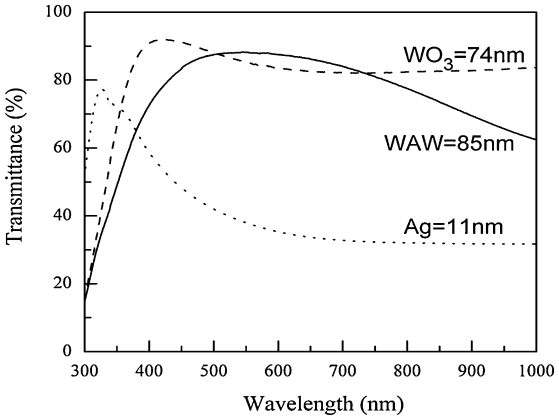

Fig. 2. Measured transmittance spectra of Ag (11 nm), WO_3 (74 nm), and WAW (85 nm).

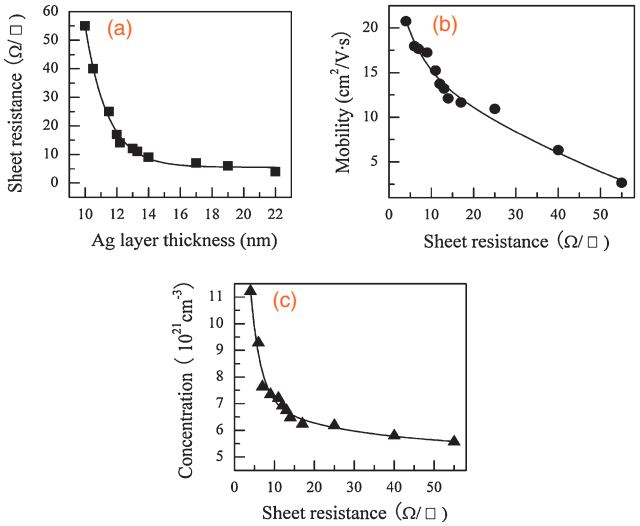

Fig. 3. (a) Sheet resistance of WAWs versus Ag layer thickness. (b) Electron mobility versus sheet resistance of WAW. (c) Electron concentration versus sheet resistance of WAW.

To investigate how the Ag layer affects WAW electrical properties, we fabricated 12 WAW samples and attempted to make two WO_3 layers approximately the same thickness. Due to experimental deviation, the first WO_3 layer was varied from 38–42 nm, and the second WO_3 layer was varied from 35–38 nm. We then varied the Ag layer thicknesses from 10–22 nm. Figure 3 shows the electrical properties of the WAWs. When the thickness of the Ag layer was less than 12 nm, WAW sheet resistance decreased dramatically from 55 to 14 Ω/sq when the thickness was increased [Fig. 3(a)]. Sheet resistance decreased slowly from 14 to 4 Ω/sq as the thickness was increased further. The dependences of the measured carrier mobility and the concentration of those samples on sheet resistance, are shown in Figs. 3(b) and 3(c), respectively. Both the mobility and concentration curves show that the rate changed quickly below 14 Ω/sq and slowly at rates above it. Therefore, 12 nm Ag thickness is the turning point for WAW electrical performance. Based on the simulation data in Fig. 1 and the experimental data in Fig. 3, we deduce that for the best

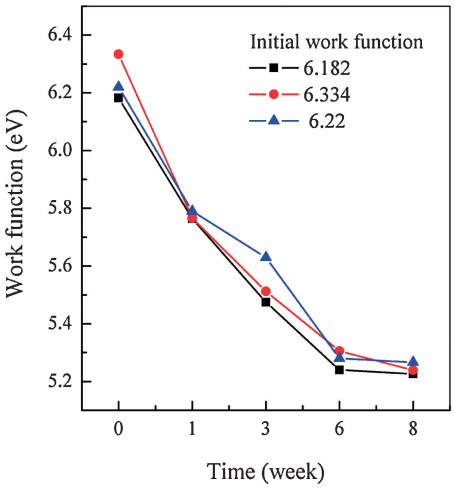

Fig. 4. Degradation of WAWs work function with time.

transmittance in the visible region, as well as for optimized electrical properties of WAWs, the thicknesses of the three layers should be from 35–45/11–15/35–45 nm.

The work function of the WAW samples was studied with a layer thickness of 38/13/35 nm. Figure 4 shows that the WAW film can have a high work function above 6.0 eV, which will decrease when exposed to ambient air. Starting with the variation of 6.182–6.334 eV, the WAW work functions eventually decrease to 5.226–5.238 eV after 8 weeks of exposure, while the sheet resistance of each sample remains the same. The change of the work function with time is probably due to the adsorption of residue gas at the WO_3 surface.[19] We observed that the work function of WAW can return to about 5.6 eV when heated at 100 °C for 30 min, which suggests that water vapor is one of the adsorbed gases at the WO_3 surface. A high work function is important for the design of electroluminescent devices and solar cells. These results suggest that WAW can be used as a suitable anode in these devices, particularly flexible ones. The effect of surface adsorption or contamination on the work function of WAW is unclear and is being studied. On the other hand, plasma treatment should be a good way to obtain a neat WAW anode in device processing.

In conclusion, multilayer transparent conductive films, $WO_3/Ag/WO_3$ with an extremely high work function of 6.334 eV, were realized under room temperature conditions. Each layer's influence on the WAW transmittance is simulated and the optimal Ag thickness is determined. It is found that the electrical properties and average transmittance of WAWs are dominated by the Ag layer thickness, while the transparent region is dependent on the two WO_3 layers.

Acknowledgments This study was supported by the CAS Innovation Program, Jilin Province Science and Technology Research Project Nos. 20090346 and 20100570, and National Science Foundation of China Nos. 51102228 and 61106057.

1) T. Kawashima, T. Ezure, K. Okada, H. Matsui, K. Goto, and N. Tanabe: J. Photochem. Photobiol. A **164** (2004) 199.
2) R. G. Gordon: MRS Bull. **25** [8] (2000) 52.
3) A. M. Al-Shukri: Desalination **209** (2007) 290.
4) D. S. Ginley and C. Bright: MRS Bull. **25** [8] (2000) 15.
5) D. W. Matson, C. C. Bonham, J. S. Swensen, L. Wang, A. Padmaperuma, D. J. Gaspar, J. J. Berry, D. S. Ginley, A. K. Sigdel, and C. W. Gorrie: Proc. SPIE **7415** (2009) 74150X.
6) S. Noguchi and H. Sakata: J. Phys. D **13** (1980) 1129.
7) D. B. Fraser: Thin Solid Films **13** (1972) 407.
8) S. A. Agnihotry, K. K. Saini, T. K. Saxena, K. C. Nagpal, and S. Chandra: J. Phys. D **18** (1985) 2087.
9) K. H. Choi, H. J. Nam, J. A. Jeong, S. W. Cho, H. K. Kim, J. W. Kang, D. G. Kim, and W. J. Cho: Appl. Phys. Lett. **92** (2008) 223302.
10) N. Wang, X. X. Liu, and X. Y. Liu: Adv. Mater. **22** (2010) 2211.
11) J. Cui, A. Wang, N. L. Edleman, J. Ni, P. Lee, N. R. Armstrong, and T. J. Marks: Adv. Mater. **13** (2001) 1476.
12) M. Kröger, S. Hamwi, J. Meyer, T. Riedl, W. Kowalsky, and A. Kahn: Org. Electron. **10** (2009) 932.
13) M. Miyazaki and E. Ando: J. Non-Cryst. Solids **178** (1994) 245.
14) S. Y. Ryu, J. H. Noh, B. H. Hwang, and S. Y. Park: Appl. Phys. Lett. **92** (2008) 023306.
15) K. S. Yook, S. O. Jeon, C. Joo, and J. Y. Lee: Appl. Phys. Lett. **94** (2009) 093501.
16) D. P. Norton: Mater. Sci. Eng. R **43** (2004) 139.
17) S. Dabbous, T. B. Nasrallah, J. Ouerfelli, K. Boubaker, M. Amlouk, and S. Belgacem: J. Alloys Compd. **487** (2009) 286.
18) D. R. Lide: *CRC Handbook of Chemistry and Physics* (CRC, Boca Raton, FL, 2008) p. 417.
19) J. Meyer, S. Hamwi, T. Bülow, H. H. Johannes, T. Riedl, and W. Kowalsky: Appl. Phys. Lett. **91** (2007) 113506.
20) C. C. Chang, S. W. Hwang, C. H. Chen, and J. F. Chen: Jpn. J. Appl. Phys. **43** (2004) 6418.
21) A. Thelen: *Design of Optical Interference Filters* (McGraw-Hill, New York, 1989) p. 9.
22) J. P. Hong, A. Y. Park, S. Lee, J. Kang, N. Shin, and D. Y. Yoon: Appl. Phys. Lett. **92** (2008) 143311.